Bioactive Materials 30 (2023) 73–84

Contents lists available at ScienceDirect

Bioactive Materials

journal homepage: www.keaipublishing.com/en/journals/bioactive-materials

Hematoma-like dynamic hydrogelation through natural glycopeptide molecular recognition for infected bone fracture repair

Shenghao Wang [a], Wenbo He [c], Huan Wang [a], Dachuan Liu [a], Miao Wang [c], Huilin Yang [a,**], Guoqing Pan [c,***], Bin Li [a,b,*]

[a] Orthopedic Institute, Department of Orthopaedic Surgery, Medical 3D Printing Center, The First Affiliated Hospital, School of Biology & Basic Medical Sciences, Suzhou Medical College, Soochow University, Suzhou, Jiangsu, 215006, China
[b] Collaborative Innovation Center of Hematology, Soochow University, Suzhou, Jiangsu, 215006, China
[c] Institute for Advanced Materials, School of Materials Science and Engineering, Jiangsu University, Zhenjiang, Jiangsu, 212013, China

ARTICLE INFO

Keywords:
Dynamic biomaterial
Molecular recognition
Hematoma mimicking
Infected fracture repair
Inflammatory microenvironment restoration

ABSTRACT

Infected bone fractures remain a major clinical challenge for orthopedic surgeons. From a tissue regeneration perspective, biomaterial scaffolds with antibacterial and osteoinductive activities are highly desired, while advanced materials capable of mimicking the pathological microenvironment during the healing process of infected tissues remain an area deserving more research. Hematoma, the gel-like blood coagulum, plays an essential role in bone fracture repair because of its ability to serve as a dynamic and temporary scaffold with cytokines for both pathogen elimination and tissue healing. In light of this, we designed a dynamic hydrogel with hematoma-like antimicrobial or reparative performance for infected bone fracture repair in this study. The proposed dynamic hydrogel network was based on the reversible recognition of a natural glycopeptide antibiotic vancomycin (Van) and its target dipeptide D-Ala-D-Ala (AA), which could serve as a hematoma-like scaffold for obliterating bacteria in the fracture region and promoting bone repair by introducing an endogenous osteogenic peptide (OGP). In vivo experiments demonstrated that the hydrogel could rapidly eradicate bacteria, improve bone regeneration and restore the local inflammatory microenvironment. Together, findings from this study imply that the use of hematoma-like dynamic hydrogel could lead to a biomimetic revolution in surgical strategies against susceptible bone fractures.

1. Introduction

Since the rise of human civilization, infected bone fractures have been a distressing and frustrating disease tormenting the global population. The first written description of osteomyelitis and rudimentary wound management for an open fracture was discovered in an Egyptian Papyrus dated 3000 BC [1]. In China, the earliest infected bone fractures were documented in the ancient Chinese medical literature of Huangdi Neijing. Intriguingly, unlike other infectious diseases that can be effectively treated over time, treatments of bone fracture-related infections have never been fully resolved. Of the 178 million new fractures occurring annually worldwide, infected bone fractures involve approximately 30% of open fractures and 2% of closed fractures [2,3], leading to an even higher global burden and impact than periprosthetic joint infections [3]. Affected individuals often face an excessive burden both physically and financially [4]. The prevalence of recurrent or persistent infections after revision surgery remains as high as 33% [5] and costs $15,000-$150,000 per capita [6,7]. Infected bone fractures are mostly acquired exogenously [3]. Staphylococcus aureus (*S. aureus*) was found to be the pathogen with the highest prevalence [8]. During the infection, *S. aureus* induces suppurative inflammation leading to tissue necrosis and destruction of bone trabeculae and bone matrix, which completely

Peer review under responsibility of KeAi Communications Co., Ltd.
* Corresponding author. Orthopedic Institute, Department of Orthopaedic Surgery, 3D Medical Printing Center, The First Affiliated Hospital, School of Biology & Basic Medical Sciences, Suzhou Medical College, Soochow University, Suzhou, Jiangsu, 215006, China.
** Corresponding author. Orthopedic Institute, Department of Orthopaedic Surgery, 3D Medical Printing Center, The First Affiliated Hospital, School of Biology & Basic Medical Sciences, Suzhou Medical College, Soochow University, Suzhou, Jiangsu, 215006, China.
*** Corresponding author.
E-mail addresses: suzhouspine@163.com (H. Yang), panguoqing@ujs.edu.cn (G. Pan), binli@suda.edu.cn (B. Li).

https://doi.org/10.1016/j.bioactmat.2023.07.018
Received 25 April 2023; Received in revised form 3 July 2023; Accepted 20 July 2023

destroys the natural bone healing process and poses a great challenge to orthopedic surgeons [9,10]. Clinical guidelines for the management of fracture infection include systemic antimicrobial therapy, rigorous debridement, local antibiotic therapy (antibiotic-laden cement or beads), and even implant removal or replacement [8,10–12]. Despite these clinical interventions, the infection risk can reach up to 50% in open fractures [13]. Thus, early diagnosis and appropriate therapies are key to effective clinical management [14–16]. If not timely cleared at an early stage, pathogenic bacteria could colonize the osteocyte lacuno-canalicular network (OLCN) and other dead spaces to form biofilms that allow residing bacteria to withstand even 1000 times the minimum inhibitory concentration of required antibiotics [5,17]. The complex nature of fracture infection indicates the multiple clinical needs for early local clearance of infecting bacteria, restoration of the inflammatory environment and maintenance of normal fracture healing. All the above situation prompts an urgent need to develop alternative strategies or newer functional materials to improve the clinical management of bone infections.

Antibacterial hydrogels are a class of emerging, attractive and highly applicable material with the potential to change the management and treatment strategies of infected bone fractures due to their potential to enhance local bacteriostatic levels [3]. However, there are several critical challenges in the design of antibacterial hydrogels for fracture-related infections [3]. First, traditional static hydrogels lack sufficient flexibility to adapt to different complex fracture scenarios and thus do not provide “full coverage” of the infected area. Second, the unplanned local release of numerous antibiotics or other antibacterial drugs does not increase antibacterial efficacy but affects the local microenvironment. Third, implanted hydrogels that excessively pursue antibacterial effects and mechanical properties often fail to achieve biomimicry, which may disrupt the local tissue microenvironment and hamper natural fracture healing. Therefore, advanced antibacterial hydrogels for the treatment of infected bone fractures should meet the above demanding requirements, such as efficient bactericidal activities to eliminate bacteria, dynamic structures to adapt defect geometry, and biomimetic properties that could recapitulate the pathological microenvironment during the fracture healing process.

Dynamic hydrogel represents one of the most promising materials for tissue engineering and regeneration medicine [18]. Due to partial similarity to extracellular matrix (ECM), such hydrogels are believed to offer distinct advantages in regulating cell-biomaterial interactions and promoting tissue and organ morphogenesis [19]. By strategically designing their dynamic features, these hydrogels have demonstrated a capacity to respond dynamically to environmental cues and biological stimuli, thereby modulating cell behaviors such as adhesion, differentiation, apoptosis and so on [20,21]. The dynamic hydrogels with precise biological effects are garnering increasing attention for their significant impact in areas such as drug-targeted therapy and tissue engineering [20].

We found that the physical properties of a typical dynamic hydrogel (e.g., the mechanical strength and the self-recovery and remoldable properties) were close to that of hematoma, a collection of clotted blood during blood vessel injuries. Hematoma plays an essential role in natural fracture healing. It can quickly form upon fracture in the early stage of the inflammatory phase during the physiological bone healing process [22,23]. From this point onwards, fracture hematoma serves as a temporary dynamic scaffold, and the fibrin network mediated by the conversion of fibrinogen aggregates confers viscoelastic properties to the perifracture hematoma [24,25], thereby facilitating cells and cytokines invasion and supporting fracture healing [22,26]. The other inflammatory cells recruited within the hematoma scaffold are the primary actors dealing with foreign microorganisms at the fracture site. When the bacteria are not eliminated in the hematoma during the early phase of fracture healing (inflammatory phase), fracture infection might become inevitable due to bacterial adhesion, escape and tissue invasion [10]. Gradually, granulation tissues rich in collagen fibers and cells replace the natural hematoma, forming a soft callus, unmineralized cartilage, and eventually a hard callus and the remodeled bone [22,23]. It has been demonstrated that the removal of hematoma could delay fracture healing [27]. However, previous antimicrobial or osteogenesis-promoting biomaterials implanted at fracture sites have often ignored this fact or even conversely impeded fracture hematoma formation. In this context, we anticipate that antibacterial hydrogels with hematoma-like properties could be used as a promising biomimetic scaffold material for efficient bactericidal and osteogenic enhancement.

To mimic the hematoma-like physical properties, including the antibacterial ability, osteogenic activity, and dynamic inner structure, in this study we reported the use of vancomycin (Van) and a dipeptide D-Ala-D-Ala (AA) in fabricating a dynamic hydrogel for the treatment of infected bone fractures. Van is a potent glycopeptide antibiotic that blocks bacterial cell wall biosynthesis by binding to the specific terminal AA dipeptide of the cell wall peptidoglycan precursor (Fig. 1A and D and Fig. S9) [28]. We exploited the reversible binding interactions between Van and AA to develop a precise and dynamic 3D network hydrogel system (Fig. 1B). In addition, the self-recovery and injectable 3D hydrogel network were co-modified with osteogenic peptide (OGP), an endogenous regulatory peptide, to regulate osteogenic differentiation and promote bone regeneration [29–31]. In this context, the dynamic hydrogel network could cover the infected fracture region with adaptive reconstruction, similar to the hematoma after fracture, thereby allowing anti-inflammatory and pro-osteogenic processes for natural and functional bone healing (Fig. 1C). We believe this 3D hematoma-like hydrogelation system with specific antimicrobial and osteogenic activities would yield keen interests for the management of fracture infection due to its ability to simulate natural fracture healing processes.

2. Results and discussion

2.1. Fabrication of hydrogel with hematoma-like properties

The formation of fracture hematoma in the early stage of the natural bone healing process serves as a temporary dynamic scaffold for active cell invasion within the fracture gap and surrounding [22]. In this study, we developed an injectable and local hematoma mimics hydrogel to clear the infection and accelerate fracture healing based on our previously reported reversible Van-AA recognition strategy [28].

By grafting Van/AA onto acrylamide and NHS double-terminated linear polyethylene glycol (PEG), we synthesized vancomycin-containing monomer (Van-M) and D-Ala-D-Ala-containing monomer (AA-M) (Fig. 1B). Van-M, AA-M and OGP were mixed with photoinitiator 2-hydroxy-40-(2-hydroxyethoxy)-2-methylpropiophenone (HHMP) in the system, and hydrogels (Van-AA-OGP hydrogels) were obtained under exposure to a UV light (365 nm) after 30 minutes. The acrylamide-based monomers (Van-M and AA-M) were specifically paired with each other, and the OGP is incorporated into the network (Fig. 1B). For optimal antimicrobial effects, the molar ratio of Van-M and AA-M was chosen at 3:1 according to our previous study [28]. The gelation of the Van-M/AA-M/OGP complex proved the successful internal linkage within the Van-AA-OGP hydrogel, in which cell-adapted micron-sized porosity was also observed and did not impede normal cell activity (Fig. 2A–B, Fig. S5).

The specific recognition and polymerization of Van-M and AA-M supported the dynamic characteristics of the Van-AA-OGP hydrogel. Next, we examined the self-healing and self-recovery properties of this hydrogel. Using a razor blade to scratch the hydrogel, we found that the scratch could be repaired within a short period of time without leaving any trace (Fig. 2D) under the microscope (Movie S1). Moreover, when the hydrogel blocks stained with/without methyl orange in sequence were placed next to each other, they glued together within 10 minutes after physical connection. It could also be stretched beyond two times its original length, demonstrating a strong self-healing property (Fig. 2I). To investigate their injectability and moldability, the hydrogels were

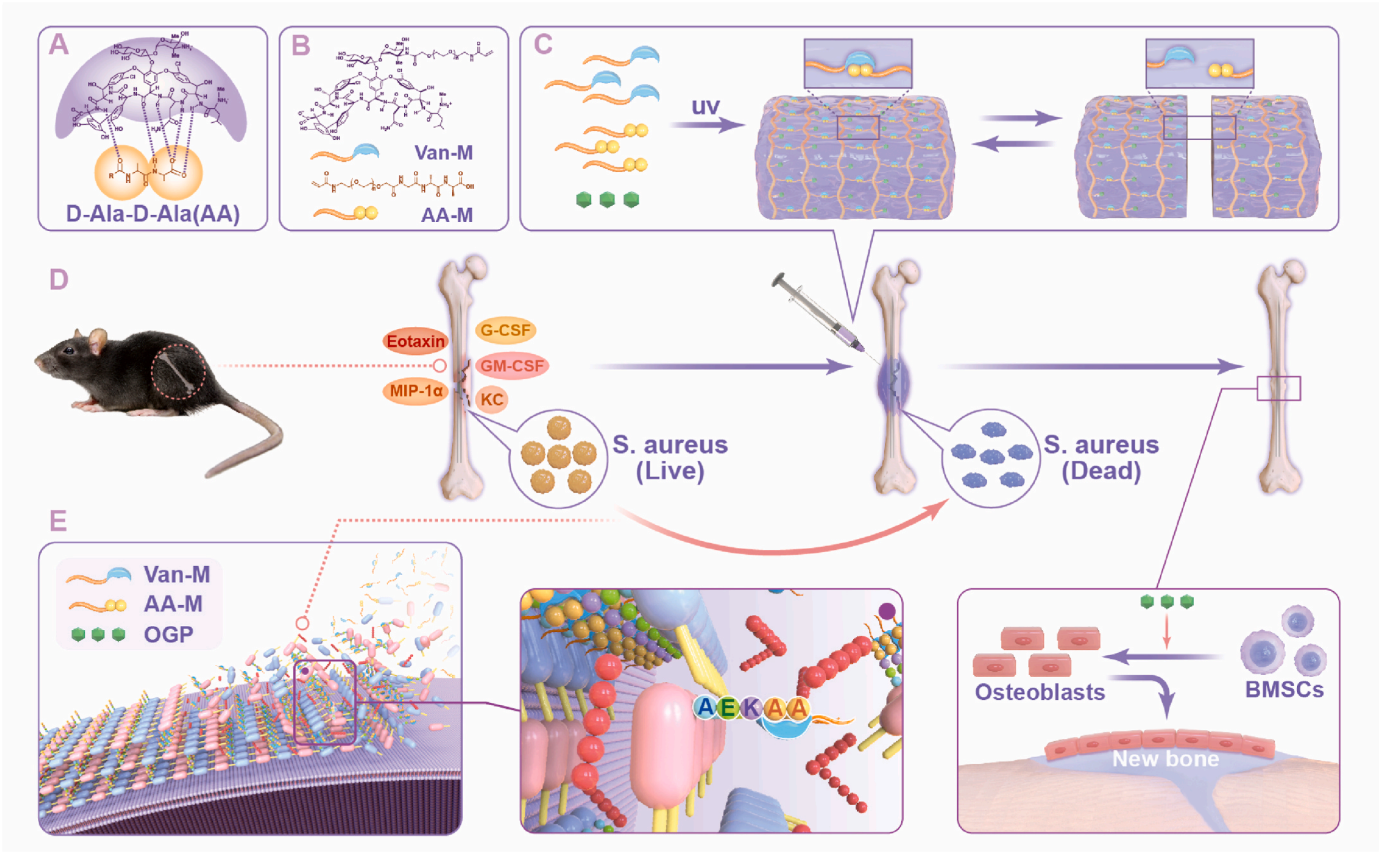

Fig. 1. Schematic overview of the synthesis and application of Van-AA-OGP hydrogel and the mechanism of bactericidal and osteogenic effects. (A) The recognition of vancomycin and specific terminal AA dipeptide of the cell wall peptidoglycan precursor in nature. (B) The molecular structure of Van-M and AA-M. (C) The synthesis and self-healing characteristics of hematoma-like Van-AA-OGP hydrogel. Van-M (marked blue) and AA-M (marked yellow) paired in the hydrogel demonstrated the reversible Van–AA interaction. (D) Schematic illustration of the Van-AA-OGP hydrogel eliminating *S. aureus* and promoting bone repair in murine fracture infection. (E) Schematic illustration of the bactericidal mechanism and osteogenic mechanism of the hematoma-like hydrogel.

extruded continuously through a 22G needle with a syringe, and found that they could be filled into the customized molds to form specific shapes (e.g., pentagram, heart) (Fig. 2E). We further investigated the viscoelasticity of Van-AA-OGP hydrogel with rheology examination. As shown in Fig. 2F, the storage modulus (G′) was greater than the loss modulus (G′′), whereby an increase in strain could collapse the dynamic structure of the hydrogel network and exhibit a crossover of G′ and G′′ (Fig. 2G). The hydrogel also showed a quick recovery from collapse in immediate switching of low-high oscillation excitation (1%–120% strain) (Fig. 2H). Interestingly, we found a similar G”/G′ in hematoma with rheology experiments, whereby the comparison of G”/G’ between the Van-AA-OGP hydrogel and hematoma showed no significance (Fig. 2J–K). This suggests that the viscoelasticity of the Van-AA-OGP hydrogel might be similar to the hematoma and could mimic hematoma-supporting cells and cytokines in bactericidal and osteogenic activities, thus could be used as a biological simulation and support for the natural healing process of fractures.

Apart from its dynamic properties, the Van-AA-OGP hydrogel also featured decent adhesiveness. The gelated hydrogel had a significantly higher adhesion force than 10% gelatin gels on both porcine skin and glass (Fig. 2L-M). Upon measuring the hydrogel degradation, we found that it could be almost degraded in 7 days (Fig. 2C). The biocompatibility was also explored, which showed that after 72 hours of coculturing with Van-AA-OGP, the mouse bone marrow stem cells (MBMSCs) maintained equivalent viability to those without coculture (Fig. 2P) and the proliferation rates of MBMSCs cocultured with/without Van-AA-OGP were similar (Fig. 2O). In addition, when Van-AA-OGP hydrogel was applied to a mouse-infected fracture model, hematoxylin and eosin (H&E) staining of mice viscera (liver, spleen, kidney and heart) sections showed no significant abnormalities between the hydrogel group and the normal group (Fig. S1).

To evaluate the antimicrobial property of the Van-AA-OGP hydrogel, we counted the colony-forming units (CFU) of *S. aureus* after incubation with monomers, Van-AA hydrogel and Van-AA-OGP hydrogel. The results exhibited significant bactericidal efficacy in mixtures containing Van-M (Van-M, Van-AA and Van-AA-OGP) (Fig. 2N, Fig. S2, Fig. S6). The results of the live/dead staining also provided evidence of the notable bactericidal properties of VAN-AA-OGP (Fig. S7B). Under scanning electron microscopy (SEM), the bacterial cell membrane of co-cultured *S. aureus* collapsed and the contents flowed out (Fig. S7A). Altogether, these results suggested that the Van-AA-OGP hydrogel has huge potential for hematoma-mimicking biocompatible biomaterial, especially for infected bone fractures.

2.2. *Hematoma-like dynamic hydrogel promotes ossification in vitro*

Osteogenesis is the natural process of healing bone fractures, and marrow stem cells are one of the four main factors in fracture healing [22,32]. To examine the osteogenesis performance of the Van-AA-OGP hydrogel, we assessed the osteogenic activity by inducing the osteogenic differentiation of MBMSCs. We examined the alkaline phosphatase (ALP) and alizarin red staining, expressions of osteogenesis-associated genes and proteins. Our results showed that 7 days after induction of osteogenic differentiation, the ALP expression of the Van-AA-OGP group was significantly upregulated, while that of the Van-AA group was slightly downregulated compared with the induced group (Fig. 3A, H).

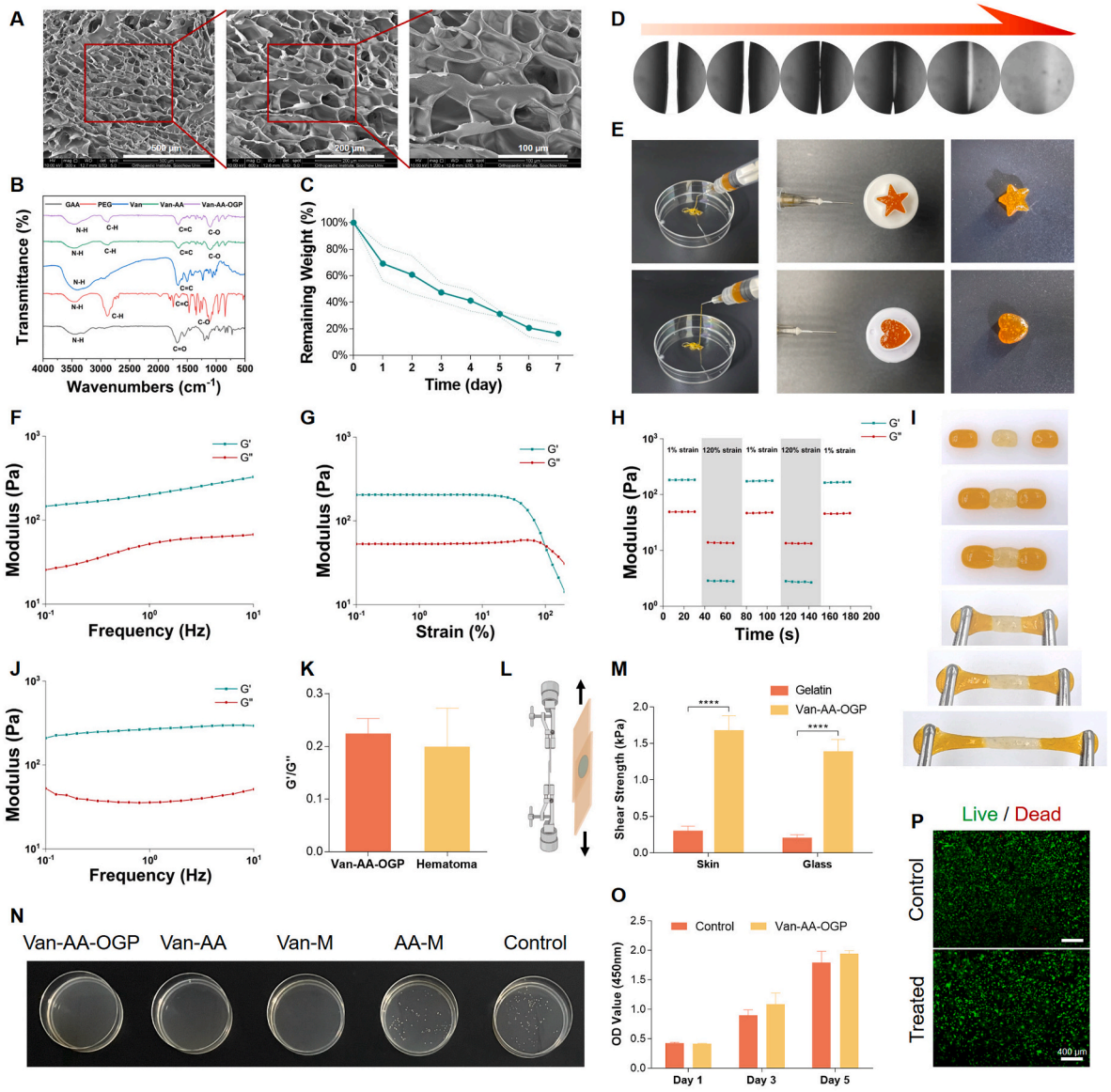

Fig. 2. Dynamic, biocompatible and bactericidal properties of the Van-AA-OGP hydrogel. (A) SEM images of Van-AA-OGP hydrogel. (B) FTIR spectra of Gaa, PEG, Van, Van-AA hydrogel and Van-AA-OGP hydrogel. (C) The hydrogel degradation rate *in vitro*. (D) The self-healing process of the scratched hydrogel. (E) The injectability of the hydrogel and the pentagram or heart shape of hydrogel injections. (F) Frequency sweeps of the hydrogel (1% strain). (G) Dynamic oscillatory strain sweeps of Van-AA-OGP hydrogel (1Hz). (H) The strain sweeps of Van-AA-OGP hydrogel (1%–120% strain at 1Hz). (I) The integration of hydrogel blocks indicated a strong self-healing property. (J) Frequency sweeps of hematoma (1Hz). (K) Comparison of G"/G′ between the Van-AA-OGP hydrogel and hematoma. (L) Schematic illustration of lap-shear test of the Van-AA-OGP hydrogel on glass and skin. (M) Comparing the adhesion force between the Van-AA-OGP hydrogel and 10% gelatin gel. (N) The CFUs of *S. aureus* were measured on LB agar after incubation with different materials, and the representative photograph was displayed. (O) The proliferation of MBMSCs cocultured with/without hydrogel was evaluated using Cell Counting Kit-8 (CCK-8). (P) Fluorescence microscopy images of live/dead staining of MBMSCs with/without coculture.

In addition, the expression of osteogenesis-related genes, such as *Col1a1*, *Spp1* and *Bglap2*, in the Van-AA-OGP group was concomitantly elevated compared with the induction-only group (Fig. 3B–D). After 14 days of osteogenic induction, bone matrix mineralization was enhanced in the Van-AA-OGP group, which was supported by the quantification analysis of alizarin red staining (Fig. 3A, I). The expression levels of *Col1a1*, *Spp1* and *Bglap2* were also promoted in the Van-AA-OGP group (Fig. 3E–G). Consistent with gene expressions, the protein expressions of RUNX2, osteopontin (OPN) and osteocalcin (OCN) exhibited a similar result, indicating a general upregulation in the Van-AA-OGP group (Fig. 3J). Overall, the Van-AA-OGP hydrogel could efficiently promote the osteogenic differentiation of MBMSCs. Together with the results of *in vitro* bactericidal efficacy of the hydrogel, this unique hydrogel was confirmed to have the dual integration of efficient anti-infection and osteogenesis promotion *in vitro*.

2.3. Hematoma-like dynamic hydrogel eliminates *S. aureus* infection from femur fracture

In clinical practice, diaphyseal fractures are usually treated by intramedullary nail fixation to align the bone fragments anatomically and obtain sufficient stability for natural bone healing. However, pathogenic bacteria could severely interfere with this process, leading to bone necrosis and reactive bone formation [33,34]. Based on reported literature, we developed a mouse fracture infection model at its femoral shaft to simulate a realistic fracture infection scenario [35]. In this model, we separately treated the infected fracture site with PBS, Van-AA hydrogel and Van-AA-OGP hydrogel, and a group with sterile femur

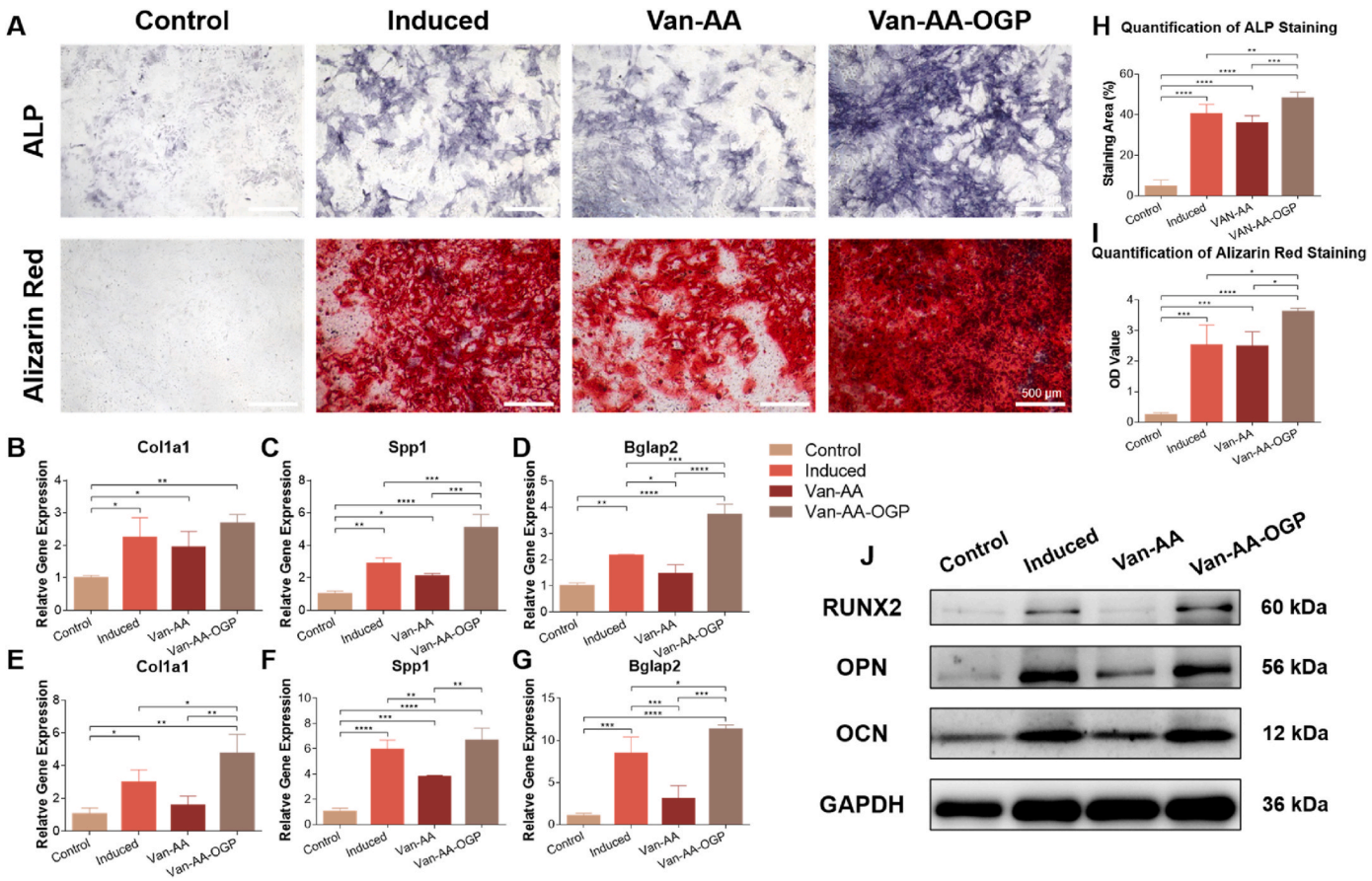

Fig. 3. Van-AA-OGP hydrogel promotes osteogenic differentiation *in vitro*. (A) The representative ALP and alizarin red staining of MBMSCs in different groups after osteogenic induction. (B) Col1a1, (C) Spp1 and (D) Bglap2 gene expressions were upregulation of MBMSCs in the Van-AA-OGP group 7 days after osteogenic differentiation. (E) Col1a1, (F) Spp1 and (G) Bglap2 gene expressions of MBMSCs were upregulated in the Van-AA-OGP group 14 days after osteogenic differentiation. (H) Quantitative analysis of ALP staining. (I) Quantitative analysis of alizarin red staining. (J) Western blot analysis of RUNX2, OPN and OCN of MBMSCs 14 days after osteogenic differentiation.

fracture was used as control. Four weeks after surgery, we analyzed the bacterial burden from the harvested tissues. The treated perifracture tissue extracts were inoculated on agar plates (Fig. 4B, Fig. S3), but no bacterial colony growth was observed between the two hydrogel-treated and the control groups. However, the agar plates of the fracture-infected group were covered with bacterial colonies. Qualification of CFUs demonstrated large numbers of recovered bacteria in the infection group, confirming the effects of long-term infection (Fig. 4C). These findings revealed the significant antimicrobial properties of Van-AA and Van-AA-OGP hydrogels *in vivo*, decreasing the pathogenic bacteria to the level of the sterile group. To further compare the antimicrobial performances of the hydrogels, we examined their corresponding histological sections at 4 weeks postoperatively. The results showed bacterial accumulations in bone crevices or compartments in the infection group via Giemsa and Gram staining (Fig. 4A). Immunofluorescence staining further confirmed the existence of *S. aureus* in the infection group (Fig. 4A), indicating a severe *S. aureus* invasion at the fracture site. The groups treated with Van-AA and Van-AA-OGP hydrogel completely eliminated the bacteria as expected, which was consistent with the control group. These strong evidences indicated that the Van-AA or Van-AA-OGP dynamic hydrogel inherited well the potent antimicrobial properties of vancomycin and displayed strong antibacterial effects *in vitro* and *in vivo*.

In clinical practice, current strategies focus on the application of systemic medications and topical antibiotic beads as a temporary filler of the dead space for local anti-infective treatment [10,36–38]. However, the probability of treatment failure remains disproportionately high [7,37,39]. Recent discoveries provide further important explanations for bacterial persistence and treatment failure by suggesting that *S. aureus* invades and colonizes the dead space or OLCN and develops biofilms for long-term infection [8,40–42]. In addition, due to the complexity of fractures and trauma, antibiotic-loaded fillers cannot perfectly adapt irregular shapes, exacerbating the dilemma of poor antibiotics penetration.

Our constructed dynamic hydrogel represents an ingenious solution to this problem because our proposed hydrogel benefits from reversibility by entering the fracture gap and surrounding structures, tightly wrapping the fracture and filling the dead space. The molecular recognition of the Van-AA structure can efficiently help identify and kill pathogenic bacteria. As a result, an immediate sufficient quantity of topical Van-AA-OGP hydrogel application can effectively sterilize and suppress cellular infectious inflammation.

2.4. *Hematoma-like dynamic hydrogel remodels the inflammatory microenvironment in the fracture healing process*

There are three distinct stages of fracture healing: inflammation, repair and remodeling [22]. Inflammation is the first and crucial stage after a fracture. It develops at the same time as hematoma formation. The inflammatory cascade is initiated by fracture-induced damage to surrounding tissues and cells [26]. Afterward, the surrounding tissue displays the typical symptoms of acute inflammation, and immune cells respond to stimuli by exerting specialized functions [23]. After a fracture, neutrophils are first recruited to the fracture site [22].

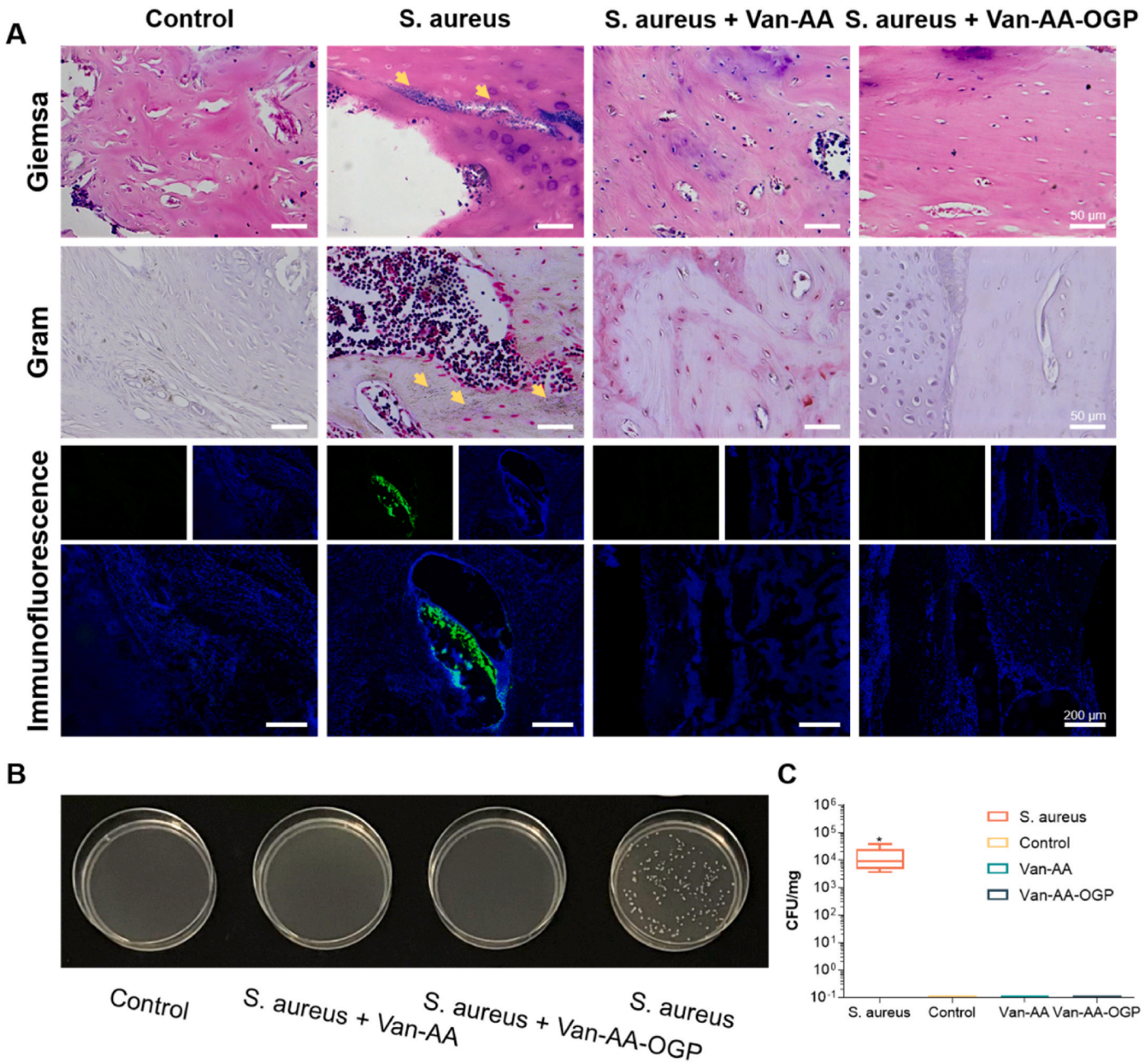

Fig. 4. Bactericidal activity of the Van-AA-OGP hydrogel *in vivo*. (A) Representative Giemsa, Gram and Immunofluorescence staining of the histological sections of murine femur isolated 4 weeks after fracture. The yellow arrows highlight the pathogenic bacteria. The separate and merged immunofluorescences showed *S. aureus* (green) with DAPI in blue. (B) The CFUs of *S. aureus* recovered from the tissues were measured on LB agar, and the representative photograph is displayed. (C) Quantitative analysis of bacterial viability was performed according to colonies on agar plates.

Subsequently, macrophages and lymphocytes migrate to the fracture callus, initiating an adaptive immune response [22]. In addition, many pro-inflammatory cytokines, including IL-1β, IL-6 and TNF, are released by activated immune cells, constituting the fracture inflammatory microenvironment [22,23]. The complex intra-network interaction of cytokines, immune cells, and mesenchymal stem cells in this inflammatory microenvironment drives the bone repair cascade, including angiogenesis and cell differentiation. The specific aggregation of immune cells and cytokines in the local temporal space of the fracture within the dynamic hematoma scaffold is an important factor in the bone healing process, with the acute inflammatory phase lasting approximately 7 days post-fracture [22,43]. However, it should also be noted that the specific immune response could negatively impact fracture healing [22,44]. Thus, there is a delicate homeostasis in the inflammatory microenvironment at the fracture site to promote bone healing; however, the specific underlying mechanism remains unclear.

Bacterial infection is a typical disruptor of this environment. It breaks the existing balance and prolongs the inflammatory phase that would otherwise end in 5–10 days [22,23]. Disruption of these finely tuned events could dramatically impact the fracture healing process [22,45,46], leading to fracture non-union and further bone destruction. To accurately identify the abnormal inflammatory microenvironment and analyze whether hydrogels have a positive and persistent impact on the inflammatory microenvironment, we treated the infected fractures with/without hydrogels, using a sterile fracture as control. We examined 23 common inflammatory cytokines using a mouse cytokine array of the tissues surrounding the fracture site 4 weeks post-surgery. Infected fracture, infected fracture treated with Van-AA hydrogel, infected

fracture treated with Van-AA-OGP hydrogel and sterile control were included in the experimental groups: The infection group exhibited a clearly different cytokine expression profile (Fig. 5A), especially in IL-3, IL-4, IL-5, IL-10, IL-12(p40), eotaxin, G-CSF, GM-CSF, KC, MIP-1α, MIP-1β and TNF-α (Fig. 5B-M), among which pro-inflammatory cytokines (G-CSF, TNF-α) and other cytokines are implicated in adaptive immunity (IL-3, IL-4, IL-5, IL-12(p40), eotaxin, GM-CSF, KC, MIP-1α and MIP-1β). Unlike the massive release of cytokines which indicated a strong inflammatory response in the infection group, there were no significant differences among the other groups. The immune cells in the tissues also support the high levels of inflammatory cytokines, where a significant $CD3^+$ T cell and $F4/80^+CD11b^+$ macrophage recruitment was observed in the infection group compared with the other groups (Fig. S4). In addition, the percentage of helper T cells ($CD3^+CD4^+$ T cells) was significantly upregulated in the infection-only group, demonstrating a typical adaptive immune response (Fig. S4A). These results revealed that the S. aureus-induced infection triggered a long-term massive concentration of cytokines recruited by perifracture inflammation, similar to the previous literature [47]. They also confirmed the adverse effects of prolonged adaptive immunity in the local inflammatory microenvironment on fracture healing. Most importantly, the non-significant difference in the Van-AA-OGP hydrogel-treated group and the control group showed rapid and complete clearance of *S. aureus* by the potent molecular recognition of hydrogel and restoration of the inflammatory environment in bone repair.

Previous studies have already indicated that, the inflammation microenvironment is closely associated with tissue injury and regeneration [48]. Tissue regeneration usually starts with acute immune-inflammatory responses at inflammatory stage, therefore determines the effectiveness of ensuing repair and remodeling [48]. Emerging studies focus on the modulation of macrophages phenotype (switch from M1 to M2), Tregs/small extracellular vesicles mediated immunomodulation or even neuroimmune regulation [48–50]. Biomaterials with microenvironmental modulation functions have shown great potential in bone/cartilage/soft tissue regeneration [48,51]. In this study, the Van-AA-OGP network showed the restoration of the inflammatory cytokines as well as the immune cells in the local microenvironment. Further investigations of the inflammatory cues may help elucidate the exact biological mechanisms.

2.5. *Hematoma-like dynamic hydrogel improves the natural healing of infected fractures*

Fracture infection often triggers local osteonecrosis and abscesses. As the infection becomes chronic, sequestrum and involucrum formation might occur, ultimately leading to the non-union of the fracture [10,33]. Previous literature demonstrated that local infection might deteriorate bone quality, leading to a progressive decrease in bone volume fraction and BMD [52–54]. Accordingly, we introduced OGP molecules into the hydrogel network for better pro-osteogenic capacity. To investigate whether hydrogels could promote fracture healing while clearing up infection, we assessed fracture healing in the fracture infection model of mice. We included the group treated with Van-AA hydrogel, Van-AA-OGP hydrogel after infection, the infection group without hydrogel treatment and the aseptic fracture group as a control. Histologic and micro-computed tomography (micro-CT) analyses were

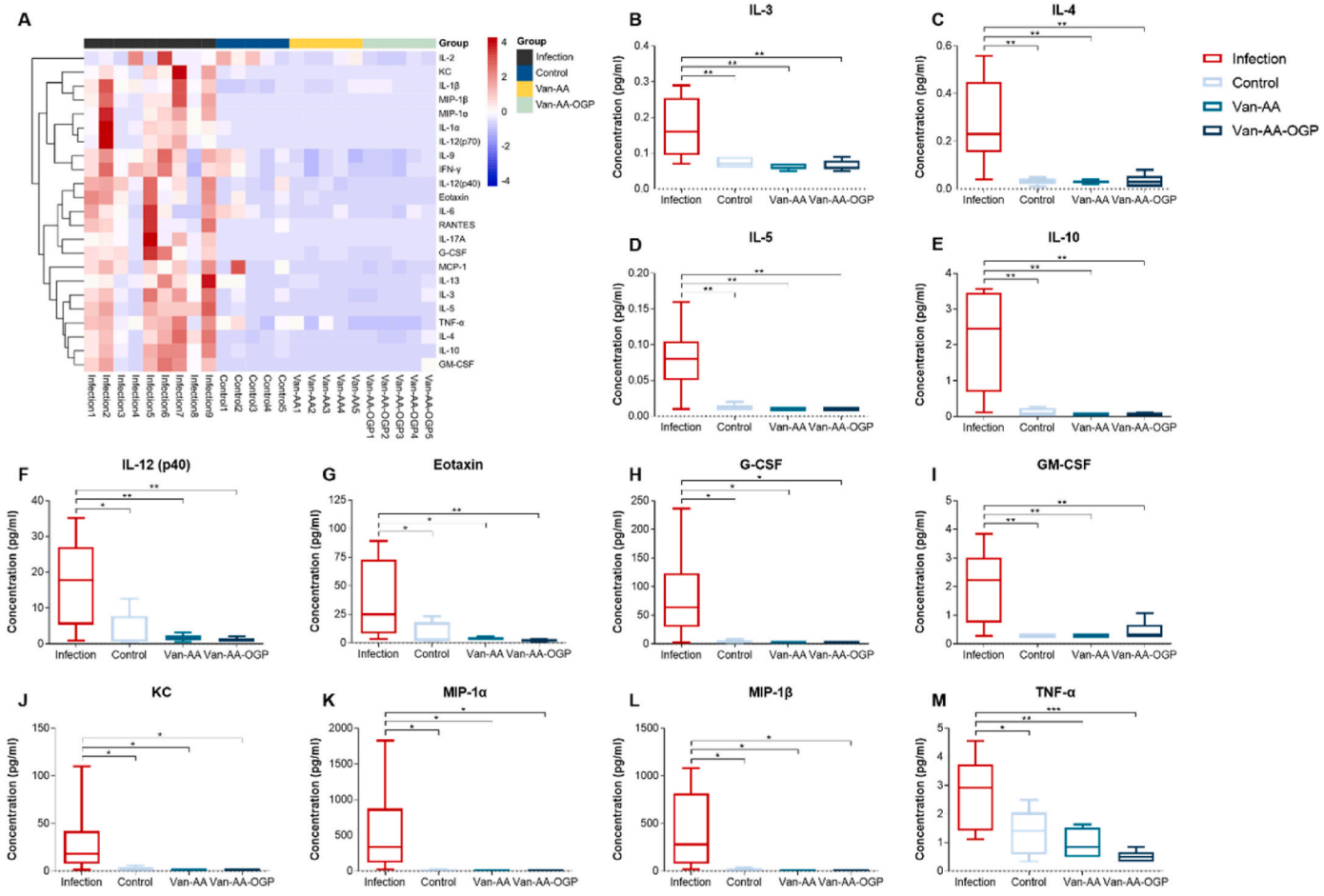

Fig. 5. Analysis of inflammatory microenvironment 4 weeks post-fracture. (A) Heatmap of the inflammatory cytokine array analysis. (B–M) Analysis of specific cytokines with significant differences (IL-3, IL-4, IL-5, IL-10, IL-12(p40), eotaxin, G-CSF, GM-CSF, KC, MIP-1α, MIP-1β and TNF-α).

conducted to monitor fracture healing at 4 and 8 weeks after fracture infection. The results showed that 4 weeks after surgery, the formation of soft to bony callus could be observed in the control group, Van-AA treated group and Van-AA-OGP treated group (Fig. 6A). However, in the infection group, there was no callus or fracture formation, but rather reactive heterotopic ossification (Fig. 6A). The infection group had the lowest bone mineral density (BMD) and bone volume (BV)/tissue volume (TV) in all groups, while the Van-AA-OGP treated group had the highest (Fig. 6D–F). Notably, there was no significant decrease in bone volume in the infection group due to reactive bone formation. H&E staining revealed a denser bone formation in the Van-AA-OGP group than in other groups, whereas bone formation in the infected group was sparse and disorganized (Fig. 6B). Masson Trichrome staining showed most new bone formation and highest bone maturation (red stained areas) in the Van-AA-OGP group during calcification in the fracture callus (Fig. 6C). The immunohistochemical staining indicated the robust expression of inducible nitric oxide synthase (iNOS) in the infection group (Fig. S8A), suggesting an excessive local inflammatory response at the fracture site. While the Van-AA-OGP group exhibited the highest level of OPN expression, as depicted in Fig. S8B, which is in agreement with previous staining results. Similar results were obtained at 8 weeks post-surgery. Micro-CT indicated that the BMD, BV and BV/TV of the Van-AA-OGP group were higher than those in the Van-AA and control group (Fig. 7D–F). We hypothesized that BV remained high in the infection group due to massive reactive ectopic osteogenesis, and the loosely organized new bone formed by the shell-like structure at the fracture site (Fig. 7A). H&E and Masson staining showed bone resorption and the formation of sequestrum (dead bone) in the infection group (Fig. 7B–C). There were no significant morphological differences in the remodeled bone formation between the Van-AA group and the control group. Comparatively, the tissue section of the Van-AA-OGP group showed denser and more fully mature new bone. The results of our hydrogel application to fractures successfully simulated the natural process of hematoma mechanization and endochondral osteogenesis, i.e., the formation of soft callus rich in chondrocytes *in situ*, which eventually transformed into hard callus. In summary, the dynamic Van-AA-OGP hydrogel could promote fracture repair and accelerate bone maturation while eradicating bacteria.

The limitation of this study was that the hydrogel was injected shortly after *S. aureus* inoculation at the fracture, which only simulated the most desirable situation in open fractures or acute fracture infections, thus urging further investigations on antimicrobial materials for complicated and chronic fracture infections. Our future studies would investigate more closely this molecular recognition hydrogel for MRSA infections as well as the development of materials for the precise regulation of the infection and inflammatory environment *in vivo*.

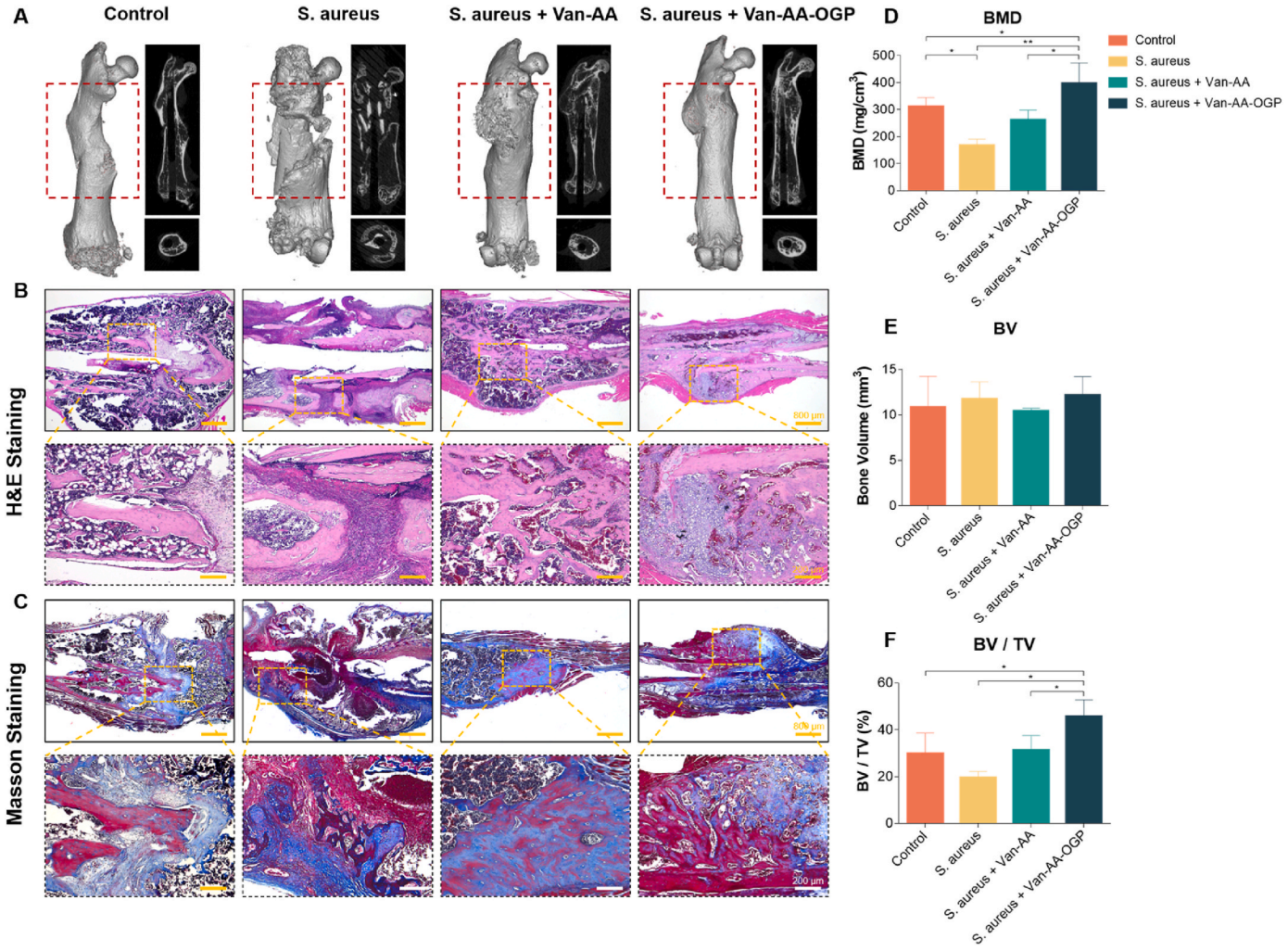

Fig. 6. Promotion of fracture healing by the Van-AA-OGP hydrogel 4 weeks post-fracture. (A) The representative micro-CT reconstructions of different groups at 4 weeks post-fracture. (B) Representative H&E staining of the murine femur in different groups. (C) Representative Masson staining of the murine femur in different groups. Quantification of BMD (D), BV (E) and BV/TV (F) from micro-CT data.

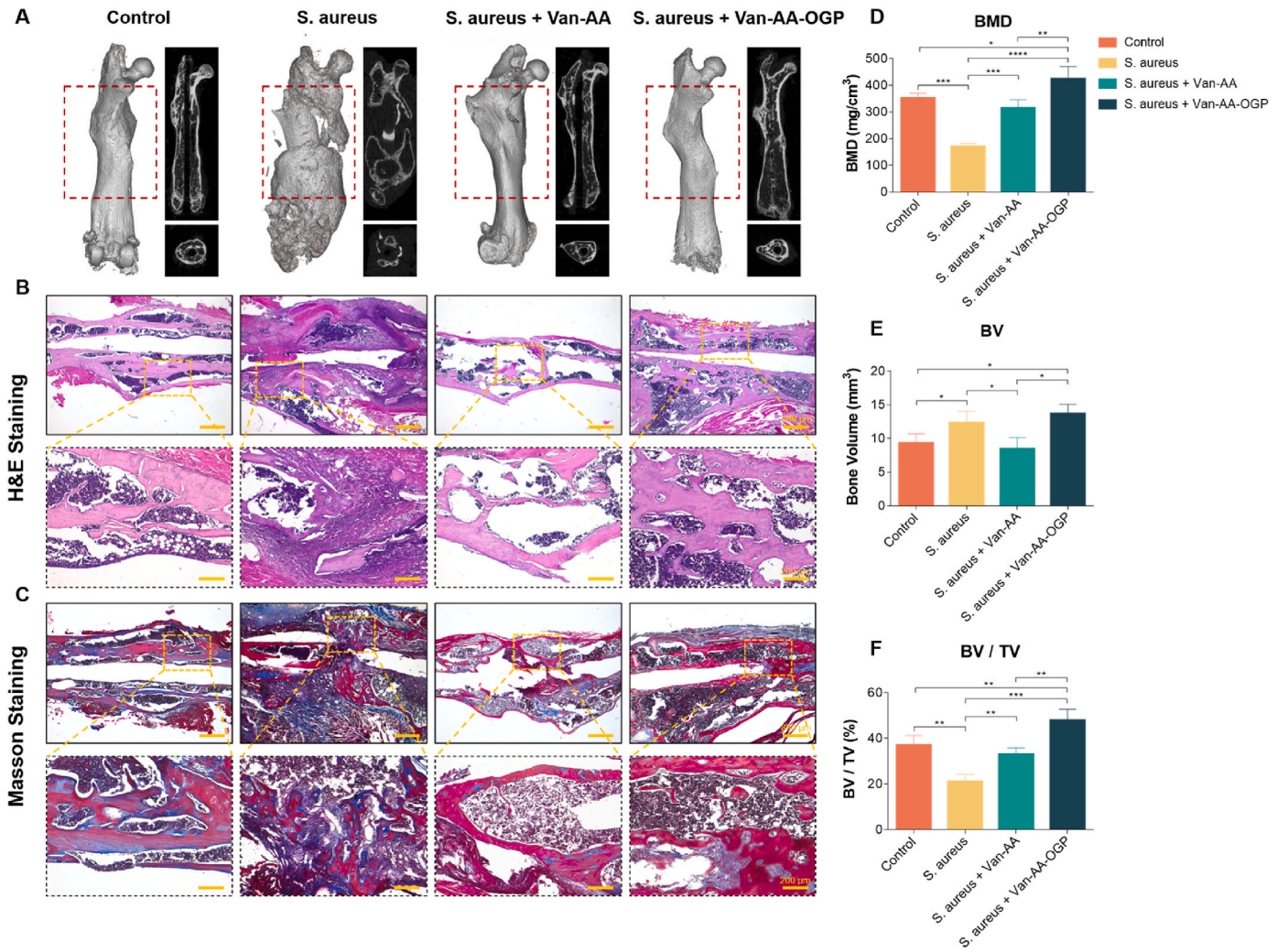

Fig. 7. Promotion of fracture healing by the Van-AA-OGP hydrogel 8 weeks post-fracture. (A) The representative micro-CT reconstructions of different groups at 8 weeks post-fracture. (B) Representative H&E staining of the murine femur in different groups. (C) Representative Masson staining of the murine femur in different groups. Quantification of BMD (D), BV (E) and BV/TV (F) from micro-CT data.

3. Conclusion

In this study, we developed a hematoma-mimicking dynamic hydrogel network using a molecular recognition strategy. The intrinsic reversible Van-AA recognition of our constructed hydrogel showed potent bactericidal properties for targeting *S. aureus*. With OGP introduced in the network, the Van-AA-OGP hydrogel also demonstrated excellent pro-osteoclastogenic capacity *in vitro*. In infected fractures, the hydrogel simulated the viscoelastic properties of hematoma, eliminated *S. aureus*, restored the inflammatory microenvironment and promoted fracture healing. We believe that deeper investigations on this hematoma-like hydrogel network with promising molecular recognition antimicrobial strategy could deepen our understanding of fracture infection and shed new light on the bactericidal biomaterials.

4. Experimental section

Materials: Vancomycin hydrochloride (Van·HCl, Aladdin), Penicillin and streptomycin (PS, Gibco, Australia), Cell Counting Kit-8 (CCK8, BBI life Science, Sangon Biotech, China), Alpha MEM (HyClone, USA), Fetal bovine serum (FBS, HyClone, USA), RNAiso Plus (Takara, China), iTaq Universal SYBR Green Supermix (Bio-Rad, USA), ascorbic acid (Sigma-Aldrich), β-glycerophosphate (Sigma-Aldrich), dexamethasone (Sigma-Aldrich), Bio-Plex Pro Mouse Cytokine 23-plex Assay (Bio-Rad, USA), iTaq Universal SYBR Green Supermix (Bio-Rad, USA), collagenase type I & II (Yeasen Biotech, China), Bio-Plex Pro Mouse Cytokine 23-plex Assay (Bio-Rad, USA), FITC anti-mouse CD3 (BioLegend), APC anti-mouse CD4 (BioLegend), PerCP/Cyanine5.5 anti-mouse CD8a (BioLegend), PE anti-mouse F4/80 (BioLegend), AlexaFluor 700 anti-mouse CD11b (BioLegend), PE/Cyanine7 anti-mouse CD206 (BioLegend), and APC/Cyanine7 anti-mouse CD86 (BioLegend). Cell viability was assessed by PE/Dazzle 594 Zombie Red Fixable Viability Kit (BioLegend), Gaa (NH2-Gly-Ala-Ala-COOH) was performed by ChinaPeptides Co, Ltd. (Shanghai, China), the acrylamide-PEG (3400)-NHS was synthesized by ToYongBio Tech.Inc. (Shanghai, China), and osteogenic growth peptide ALKRQGRTLYGFGG (OGP) was synthesized by ChinaPeptides Co, Ltd. (Shanghai, China).

Hydrogel preparation: Van-M and AA-M were prepared as described previously [28]. Briefly, Van-M was synthesized by Van (165 mg, 0.11 mmol) and acrylamide-PEG (3400)-NHS (360 mg, 0.1 mmol) in 5 ml DMSO solution. After adjusting the pH to 8.2, the dispersion was stirred at 25 °C for 24 h under argon. The mixture was dialyzed for 5 days to remove unreacted molecules, and the product was then lyophilized to yield powder. A similar procedure was used to prepare AA-M, whereby Gaa (26 mg, 0.02 mmol) and acrylamide-PEG (3400)-NHS (360 mg, 0.1 mmol) were dissolved in 4 ml mixed solution of DMSO and water (v/v = 1:1). The mixture was subsequently dialyzed and lyophilized as well. All obtained powders were stored at −20 °C.

The photopolymerizations of Van-AA-OGP hydrogels were initiated by 2-hydroxy-40-(2-hydroxyethoxy)-2-methylpropiophenone (HHMP) in Van-M/AA-M solution. Briefly, 51 mg Van-M and 12 mg AA-M were dissolved in 450 μl ultrapure water to obtain a Van-M/AA-M molar ratio of 3:1. The solution was then supplemented with OGP to achieve a final concentration of 0.7 mM. After adding 5 mg HHMP, the solution was homogenized by stirring and subsequently exposed to UV light (365 nm) for 30 min at room temperature. and the solution was exposed to UV light (365 nm) for 30 min at room temperature. Van-AA hydrogels were prepared by the same procedure, with the exception of omitting the addition of OGP.

Material characterizations: Fourier-transform infrared spectroscopy data of the monomers were recorded with an Infrared Spectrometer (FTIR, Tensor 27, Bruker, Germany). The synthesized monomers were characterized by ^{1}H NMR with a Bruker DRX500 spectrometer (Bruker, MA). Images of the lyophilized hydrogels were obtained from SEM (S-4800, Hitachi, Kyoto, Japan). The degradation test was performed in PBS at 37 °C, the lyophilized weight of hydrogel was recorded at specific time. The rheological properties of hydrogels were measured by a Discovery Hybrid Rheometer (HR2, TA Instrument, USA). Dynamic oscillatory strain sweep was conducted with the amplitude 0.1–500% at 1Hz, followed by a frequency sweep (0.1–10 Hz at 1% strain). The self-healing properties were investigated between 1% and 120% strain at 1 Hz. The self-healing properties were also assessed under a microscope by monitoring the healing process of scratched hydrogels. To further explore the performance, two pieces of the hydrogels were placed adjacent to each other on plastic slides. The self-healing process was recorded without any external force. To evaluate injectability, 500 μl hydrogel was loaded into a single syringe and injected into a custom-made model through a 22G needle. The adhesion force was measured by lap-shear tests with glass and skin using a universal mechanical testing system (HY-0580, Shanghai Hengyi, China). The hydrogel was spread onto the surface of materials (glass or skin) and covered with another piece of the same material. The bonding area had a 15 mm diameter square circle. After preloading at 1 N for 20 s, the composite structure was fixed between two claps and pulled apart in parallel at a speed of 10 mm/min.

Cytotoxicity test: MBMSCs were seeded onto 96 well plates for cell proliferation assay. After culturing in medium for 1, 3 and 5 days, cell proliferation was evaluated by CCK8. Absorbance was read by a microplate reader (BioTek, Winooski, VT, USA) at 450 nm. Live/Dead staining was also used to evaluate the cytocompatibility. Images were obtained using a fluorescence microscope (Zeiss Axiovert 200, Carl Zeiss Inc, Thornwood, NY).

In vitro antibacterial property test: The antibacterial activity of hydrogels and monomer Van-M and AA-M were evaluated similarly to previous publications [28,55]. Briefly, *S. aureus* was cultured in Luria-Bertani (LB) medium by shaking at 37 °C overnight. The concentration of bacteria in the solution was determined according to previous literature [56]. A bacteria solution (10^4 CFU/ml) was mixed with Van-M (20 mM), AA-M (6 mM), Van-AA hydrogel (20 mM) and Van-AA-OGP hydrogel (20 mM) in a 1:1 vol ratio, respectively. The mixture was incubated at 37 °C for 24 h in a shaker. Subsequently, 20 μl of the mixture was spread on a solid LB agarose medium. The CFUs were counted after overnight incubation at 37 °C.

Cell culture and differentiation test: MBMSCs were extracted from the femurs, and cultured in Alpha MEM supplemented with 10% FBS, 1% penicillin and streptomycin. The third passage of MBMSCs was used in all experiments. At day 7, osteogenic differentiation was induced by 50 μg/ml ascorbic acid, 10 mM β-glycerophosphate and 100 nM dexamethasone. The medium of different groups was changed every 3 days. ALP and Alizarin red S staining was used to confirm the osteogenic differentiation of different groups, respectively. Osteogenesis-related gene expressions were quantified by real-time PCR.

Quantitative real-time PCR analysis: The total RNA was extracted from MBMSCs using RNAiso Plus. Quantitative real-time PCR was performed using the iTaq Universal SYBR Green Supermix. The quantification of relative gene expression was normalized to GAPDH using the $2^{-\Delta\Delta Ct}$ method. All primers used in PCR were synthesized by Sangon Biotech, Shanghai, China.

Western blot: MBMSCs were harvested at particular time points for protein extraction. Levels of osteogenic proteins were analyzed with western blot according to standard protocol, GAPDH was used as a loading control.

In vivo murine femur fracture infection model: All Animal experiments were approved by the Ethics Committee of Soochow University (SUDA20220711A08). Briefly, 10-12 weeks-old C57 mice were anesthetized with sodium pentobarbital. Their left hind leg was shaved and disinfected with iodine, followed by 70% ethanol. A lateral skin incision in the left thigh and the femur shaft was exposed by blunt muscle dissection. A 22G needle was inserted into the marrow cavity along the long axis, and after the needle was removed, a femoral diaphysis fracture was created using a custom-made three-point bend instrument. The needle was inserted back into the femur to stabilize the fracture. The distal part of the needle was cut to avoid damage to the knee joint. *S. aureus* were inoculated onto the fracture site (2 μl, 10^4 CFU per mouse) to create the femur fracture infection model, and an equal volume of PBS was used at the fracture site in the control group. For mice with hydrogels injection, 15 μl Van-AA/Van-AA-OGP hydrogels were injected to cover the fracture region. After suturing back the muscle layer and closing the skin incision, the surgical area was disinfected again. All mice were placed on a homeothermic blanket until they recovered from anesthesia.

In vivo cytokine array analysis: Four weeks after fracture infection, the surrounding tissues of the fractured region were isolated. Samples were ground and homogenized before sonication. The supernatant was used for subsequent experiments. The Bio-Plex Pro Mouse Cytokine 23-plex Assay (Bio-Rad, CA, USA) was used in cytokine array analysis following the manufacturer's protocol. Briefly, the samples were incubated in 96-well plates for 30 min, followed by incubation with diluted detection antibody for 30 min, and incubated with diluted streptavidin-PE for 10 min. The data were acquired in the Bio-Plex MAGPIX System.

Flow cytometry assay for tissue samples: The perifracture tissue was isolated from mice 4 weeks post-surgery, and the tissues were minced and digested with collagenase type I and collagenase type II (1 mg/ml) for 1 hour at 37 °C. The single-cell suspensions were obtained using a cell strainer. According to the manufacturer's instructions, the suspension samples were stained and analyzed on Attune NxT Cytometer (Thermo Fisher Scientific) using the following antibodies: FITC anti-mouse CD3, APC anti-mouse CD4, PerCP/Cyanine5.5 anti-mouse CD8a, PE anti-mouse F4/80, AlexaFluor 700 anti-mouse CD11b, PE/Cyanine7 anti-mouse CD206, and APC/Cyanine7 anti-mouse CD86. Cell viability was assessed using a PE/Dazzle 594 Zombie Red Fixable Viability Kit.

Bacteria recovery from tissue samples: The mice were sacrificed 4 weeks after surgery. After skin sterilization, their femur shaft and surrounding tissues were extracted via a lateral skin incision. The needle was withdrawn, and the tissue surrounding the fractured region was separated on ice, weighed and homogenized. The tissue extracts were diluted with an LB medium. Then, 20 μl dilution was spread onto the LB agar plates and cultured overnight. Colonies were counted and normalized to tissue weight to assess the antibacterial efficiency *in vivo*.

Micro-CT analysis: At specified time points, the mice were sacrificed. After perfusion with PBS, the femora were dissected, and the needles were removed for micro-CT scanning (SkyScan 1176, Aartselaar, Belgium) at 9 μm resolution. The region of interest (ROI) was specified as a 5.3 mm long section centered on the middle of the fracture region to access its healing. Parameters including BV, Bone volume fraction (BV/TV) and BMD were analyzed using CTAn (SkyScan, Aartselaar, Belgium).

Histological evaluation: Femora were isolated from the sacrificed mice, and the needles were carefully removed from the bone marrow

cavity. All harvested femora and surrounding tissues were fixed in 10% formalin, decalcified by 10% EDTA, then embedded in paraffin [57]. The samples were sliced into 6 μm sections for H&E, Masson, Gram, immunofluorescent and immunohistochemical staining following the manufacturer's protocol. Sections were photographed using a fluorescence microscope (Carl Zeiss Inc, Thornwood, NY).

Statistical analysis: The values are represented as means ± standard deviation. The student's t-test was performed to compare the differences between two groups, and a one-way analysis of variance followed by Tukey's test was performed to make multiple comparisons. The SPSS 25.0 software was used for statistical analysis. A value of $p < 0.05$ was used to define statistical significance.

CRediT authorship contribution statement

Shenghao Wang: Conceptualization, Methodology, Writing – original draft, Writing – review & editing, Funding acquisition. **Wenbo He:** Conceptualization, Methodology, Validation, Formal analysis, Writing – review & editing. **Huan Wang:** Investigation, Formal analysis, Methodology, Validation. **Dachuan Liu:** Validation, Formal analysis, Methodology. **Miao Wang:** Investigation, Validation, Formal analysis. **Huilin Yang:** Conceptualization, Methodology, Writing – review & editing. **Guoqing Pan:** Conceptualization, Writing – review & editing, Supervision, Project administration, Funding acquisition. **Bin Li:** Conceptualization, Writing – review & editing, Supervision, Project administration, Funding acquisition.

Declaration of competing interest

The authors declare that they have no known competing financial interests or personal relationships that could appear to influence the work reported in this paper.

Acknowledgements

This work was supported by the National Natural Science Foundation of China (32222041, 82102619, 81925027, 21875092), the Natural Science Foundation of Jiangsu Province (BK20220059), the National Key Research and Development Program of China (2019YFA0112000), the Innovation and Entrepreneurship Program of Jiangsu Province, the "Jiangsu Specially-Appointed Professor" Program, and the Priority Academic Program Development (PAPD) of Jiangsu Higher Education Institutions. In addition, the authors wish to acknowledge Wayen Biotechnology for the help in cytokines array analysis and Figdraw for drawing the schematics.

Appendix A. Supplementary data

Supplementary data to this article can be found online at https://doi.org/10.1016/j.bioactmat.2023.07.018.

References

[1] J.H. Breasted, The Edwin Smith Surgical Papyrus: Published in Facsimile and Hieroglyphic Transliteration with Translation and Commentary in Two Volumes, vol. 2, University of Chicago Oriental Institute Publications, Chicago, 1930.
[2] S. Baertl, W.J. Metsemakers, M. Morgenstern, V. Alt, R.G. Richards, T.F. Moriarty, K. Young, Fracture-related infection, Bone Joint Res 10 (6) (2021) 351–353.
[3] T.F. Moriarty, W.J. Metsemakers, M. Morgenstern, M.I. Hofstee, A. Vallejo Diaz, J. E. Cassat, B. Wildemann, M. Depypere, E.M. Schwarz, R.G. Richards, Fracture-related infection, Nat. Rev. Dis. Prim. 8 (1) (2022) 67.
[4] C.H. Zhou, Y. Ren, H.J. Song, A.A. Ali, X.Q. Meng, L. Xu, H.A. Zhang, J. Fang, C. H. Qin, One-stage debridement and bone transport versus first-stage debridement and second-stage bone transport for the management of lower limb post-traumatic osteomyelitis, J Orthop Translat 28 (2021) 21–27.
[5] E.A. Masters, R.P. Trombetta, K.L. de Mesy Bentley, B.F. Boyce, A.L. Gill, S.R. Gill, K. Nishitani, M. Ishikawa, Y. Morita, H. Ito, S.N. Bello-Irizarry, M. Ninomiya, J. D. Brodell Jr., C.C. Lee, S.P. Hao, I. Oh, C. Xie, H.A. Awad, J.L. Daiss, J.R. Owen, S. L. Kates, E.M. Schwarz, G. Muthukrishnan, Evolving concepts in bone infection: redefining "biofilm", "acute vs. chronic osteomyelitis", "the immune proteome" and "local antibiotic therapy", Bone Res 7 (2019) 20.
[6] R.O. Darouiche, Treatment of infections associated with surgical implants, N. Engl. J. Med. 350 (14) (2004) 1422–1429.
[7] E.M. Schwarz, J. Parvizi, T. Gehrke, A. Aiyer, A. Battenberg, S.A. Brown, J. J. Callaghan, M. Citak, K. Egol, G.E. Garrigues, M. Ghert, K. Goswami, A. Green, S. Hammound, S.L. Kates, A.C. McLaren, M.A. Mont, S. Namdari, W.T. Obremskey, R. O'Toole, S. Raikin, C. Restrepo, B. Ricciardi, K. Saeed, J. Sanchez-Sotelo, N. Shohat, T. Tan, C.P. Thirukumaran, B. Winters, 2018 international consensus meeting on musculoskeletal infection: research priorities from the general assembly questions, J. Orthop. Res. 37 (5) (2019) 997–1006.
[8] E.A. Masters, B.F. Ricciardi, K.L.M. Bentley, T.F. Moriarty, E.M. Schwarz, G. Muthukrishnan, Skeletal infections: microbial pathogenesis, immunity and clinical management, Nat. Rev. Microbiol. 20 (7) (2022) 385–400.
[9] S.W. Jung, S.H. Oh, I.S. Lee, J.H. Byun, J.H. Lee, In situ gelling hydrogel with antibacterial activity and bone healing property for treatment of osteomyelitis, Tissue Eng Regen Med 16 (5) (2019) 479–490.
[10] D.P. Lew, F.A. Waldvogel, Osteomyelitis, Lancet 364 (9431) (2004) 369–379.
[11] F. Investigators, B. Petrisor, X. Sun, M. Bhandari, G. Guyatt, K.J. Jeray, S. Sprague, S. Tanner, E. Schemitsch, P. Sancheti, J. Anglen, P. Tornetta, M. Bosse, S. Liew, S. Walter, Fluid lavage of open wounds (FLOW): a multicenter, blinded, factorial pilot trial comparing alternative irrigating solutions and pressures in patients with open fractures, J. Trauma 71 (3) (2011) 596–606.
[12] E. Steijvers, A. Ghei, Z. Xia, Manufacturing artificial bone allografts: a perspective, Biomater Transl 3 (1) (2022) 65–80.
[13] C.G. Zalavras, M.J. Patzakis, P.D. Holtom, R. Sherman, Management of open fractures, Infect. Dis. Clin. 19 (4) (2005) 915–929.
[14] C.G. Zalavras, Prevention of infection in open fractures, Infect. Dis. Clin. 31 (2) (2017) 339–352.
[15] Y. Chang, M. Bhandari, K.L. Zhu, R.D. Mirza, M. Ren, S.A. Kennedy, A. Negm, N. Bhatnagar, F.N. Naji, L. Milovanovic, Y. Fei, A. Agarwal, R. Kamran, S.M. Cho, S. Schandelmaier, L. Wang, L. Jin, S. Hu, Y. Zhao, L.C. Lopes, M. Wang, B. Petrisor, B. Ristevski, R.A.C. Siemieniuk, G.H. Guyatt, Antibiotic prophylaxis in the management of open fractures: a systematic survey of current practice and recommendations, JBJS Rev 7 (2) (2019) e1.
[16] A. Glaudemans, P.C. Jutte, M.A. Cataldo, V. Cassar-Pullicino, O. Gheysens, O. Borens, A. Trampuz, K. Wortler, N. Petrosillo, H. Winkler, A. Signore, L. M. Sconfienza, Consensus document for the diagnosis of peripheral bone infection in adults: a joint paper by the EANM, EBJIS, and ESR (with ESCMID endorsement), Eur. J. Nucl. Med. Mol. Imag. 46 (4) (2019) 957–970.
[17] P.S. Stewart, J.W. Costerton, Antibiotic resistance of bacteria in biofilms, Lancet 358 (9276) (2001) 135–138.
[18] S. Talebian, M. Mehrali, N. Taebnia, C.P. Pennisi, F.B. Kadumudi, J. Foroughi, M. Hasany, M. Nikkhah, M. Akbari, G. Orive, A. Dolatshahi-Pirouz, Self-healing hydrogels: the next paradigm shift in tissue engineering? Adv. Sci. 6 (16) (2019), 1801664.
[19] W. Li, Z. Yan, J. Ren, X. Qu, Manipulating cell fate: dynamic control of cell behaviors on functional platforms, Chem. Soc. Rev. 47 (23) (2018) 8639–8684.
[20] Y. Ma, X. Tian, L. Liu, J. Pan, G. Pan, Dynamic synthetic biointerfaces: from reversible chemical interactions to tunable biological effects, Acc. Chem. Res. 52 (6) (2019) 1611–1622.
[21] J. Robertus, W.R. Browne, B.L. Feringa, Dynamic control over cell adhesive properties using molecular-based surface engineering strategies, Chem. Soc. Rev. 39 (1) (2010) 354–378.
[22] L. Claes, S. Recknagel, A. Ignatius, Fracture healing under healthy and inflammatory conditions, Nat. Rev. Rheumatol. 8 (3) (2012) 133–143.
[23] T.A. Einhorn, L.C. Gerstenfeld, Fracture healing: mechanisms and interventions, Nat. Rev. Rheumatol. 11 (1) (2015) 45–54.
[24] A.J. Aho, Electron microscopic and histological observations on fracture repair in young and old rats, Acta Pathol. Microbiol. Scand. (Suppl 184) (1966) 181–195.
[25] M.W. Mosesson, Fibrinogen and fibrin structure and functions, J. Thromb. Haemostasis 3 (8) (2005) 1894–1904.
[26] P. Kolar, K. Schmidt-Bleek, H. Schell, T. Gaber, D. Toben, G. Schmidmaier, C. Perka, F. Buttgereit, G.N. Duda, The early fracture hematoma and its potential role in fracture healing, Tissue Eng. B Rev. 16 (4) (2010) 427–434.
[27] Y. Yang, Y. Xiao, Biomaterials regulating bone hematoma for osteogenesis, Adv Healthc Mater (2020), e2000726.
[28] W.B. He, J.X. Bai, X. Chen, D. Suo, S.H. Wang, Q.P. Guo, W.L. Yin, D.C. Geng, M. Wang, G.Q. Pan, X. Zhao, B. Li, Reversible dougong structured receptor-ligand recognition for building dynamic extracellular matrix mimics, P Natl Acad Sci USA 119 (8) (2022), e2117221119.
[29] W. Tang, G.M. Policastro, G. Hua, K. Guo, J. Zhou, C. Wesdemiotis, G.L. Doll, M. L. Becker, Bioactive surface modification of metal oxides via catechol-bearing modular peptides: multivalent-binding, surface retention, and peptide bioactivity, J. Am. Chem. Soc. 136 (46) (2014) 16357–16367.
[30] K.S. Stakleff, F. Lin, L.A. Smith Callahan, M.B. Wade, A. Esterle, J. Miller, M. Graham, M.L. Becker, Resorbable, amino acid-based poly(ester urea)s crosslinked with osteogenic growth peptide with enhanced mechanical properties and bioactivity, Acta Biomater. 9 (2) (2013) 5132–5142.
[31] M. Li, J. Bai, H. Tao, L. Hao, W. Yin, X. Ren, A. Gao, N. Li, M. Wang, S. Fang, Y. Xu, L. Chen, H. Yang, H. Wang, G. Pan, D. Geng, Rational integration of defense and repair synergy on PEEK osteoimplants via biomimetic peptide clicking strategy, Bioact. Mater. 8 (2022) 309–324.
[32] P.V. Giannoudis, T.A. Einhorn, D. Marsh, Fracture healing: the diamond concept, Injury 38 (Suppl 4) (2007) S3–S6.

[33] K.L. Urish, J.E. Cassat, Staphylococcus aureus osteomyelitis: bone, bugs, and surgery, Infect. Immun. 88 (7) (2020), e00932-00919.
[34] J.H. Calhoun, M.M. Manring, M. Shirtliff, Osteomyelitis of the long bones, Semin. Plast. Surg. 23 (2) (2009) 59–72.
[35] C.T. Johnson, J.A. Wroe, R. Agarwal, K.E. Martin, R.E. Guldberg, R.M. Donlan, L. F. Westblade, A.J. Garcia, Hydrogel delivery of lysostaphin eliminates orthopedic implant infection by Staphylococcus aureus and supports fracture healing, Proc. Natl. Acad. Sci. U. S. A. 115 (22) (2018) E4960–E4969.
[36] C. Guarch-Perez, B. Shaqour, M. Riool, B. Verleije, K. Beyers, C. Vervaet, P. Cos, S. A.J. Zaat, 3D-Printed gentamicin-releasing poly-epsilon-caprolactone composite prevents fracture-related Staphylococcus aureus infection in mice, Pharmaceutics 14 (7) (2022) 1363.
[37] A.R. Zelmer, R. Nelson, K. Richter, G.J. Atkins, Can intracellular Staphylococcus aureus in osteomyelitis be treated using current antibiotics? A systematic review and narrative synthesis, Bone Res 10 (1) (2022) 53.
[38] K.V. Brown, J.A. Walker, D.S. Cortez, C.K. Murray, J.C. Wenke, Earlier debridement and antibiotic administration decrease infection, J. Surg. Orthop. Adv. 19 (1) (2010) 18–22.
[39] W.J. Metsemakers, R. Kuehl, T.F. Moriarty, R.G. Richards, M.H.J. Verhofstad, O. Borens, S. Kates, M. Morgenstern, Infection after fracture fixation: current surgical and microbiological concepts, Injury 49 (3) (2018) 511–522.
[40] K.L. de Mesy Bentley, R. Trombetta, K. Nishitani, S.N. Bello-Irizarry, M. Ninomiya, L. Zhang, H.L. Chung, J.L. McGrath, J.L. Daiss, H.A. Awad, S.L. Kates, E. M. Schwarz, Evidence of Staphylococcus aureus deformation, proliferation, and migration in canaliculi of live cortical bone in murine models of osteomyelitis, J. Bone Miner. Res. 32 (5) (2017) 985–990.
[41] K.L. de Mesy Bentley, A. MacDonald, E.M. Schwarz, I. Oh, Chronic osteomyelitis with Staphylococcus aureus deformation in submicron canaliculi of osteocytes: a case report, JBJS Case Connect 8 (1) (2018) e8.
[42] K. Svensson Malchau, J. Tillander, M. Zaborowska, M. Hoffman, I. Lasa, P. Thomsen, H. Malchau, O. Rolfson, M. Trobos, Biofilm properties in relation to treatment outcome in patients with first-time periprosthetic hip or knee joint infection, J Orthop Translat 30 (2021) 31–40.
[43] I.H. Kalfas, Principles of bone healing, Neurosurg. Focus 10 (4) (2001) E1.
[44] D. Toben, I. Schroeder, T. El Khassawna, M. Mehta, J.E. Hoffmann, J.T. Frisch, H. Schell, J. Lienau, A. Serra, A. Radbruch, G.N. Duda, Fracture healing is accelerated in the absence of the adaptive immune system, J. Bone Miner. Res. 26 (1) (2011) 113–124.
[45] A. Wallace, T.E. Cooney, R. Englund, J.D. Lubahn, Effects of interleukin-6 ablation on fracture healing in mice, J. Orthop. Res. 29 (9) (2011) 1437–1442.
[46] L.C. Gerstenfeld, T.J. Cho, T. Kon, T. Aizawa, A. Tsay, J. Fitch, G.L. Barnes, D. T. Graves, T.A. Einhorn, Impaired fracture healing in the absence of TNF-alpha signaling: the role of TNF-alpha in endochondral cartilage resorption, J. Bone Miner. Res. 18 (9) (2003) 1584–1592.
[47] C.T. Johnson, M.C.P. Sok, K.E. Martin, P.P. Kalelkar, J.D. Caplin, E.A. Botchwey, A. J. Garcia, Lysostaphin and BMP-2 co-delivery reduces S. aureus infection and regenerates critical-sized segmental bone defects, Sci. Adv. 5 (5) (2019), eaaw1228.
[48] Y. Xiong, B.B. Mi, Z. Lin, Y.Q. Hu, L. Yu, K.K. Zha, A.C. Panayi, T. Yu, L. Chen, Z. P. Liu, A. Patel, Q. Feng, S.H. Zhou, G.H. Liu, The role of the immune microenvironment in bone, cartilage, and soft tissue regeneration: from mechanism to therapeutic opportunity, Mil Med Res 9 (1) (2022) 65.
[49] R. Tao, B. Mi, Y. Hu, S. Lin, Y. Xiong, X. Lu, A.C. Panayi, G. Li, G. Liu, Hallmarks of peripheral nerve function in bone regeneration, Bone Res 11 (1) (2023) 6.
[50] S.K. Chow, C.H. Wong, C. Cui, M.M. Li, R.M.Y. Wong, W.H. Cheung, Modulating macrophage polarization for the enhancement of fracture healing, a systematic review, J Orthop Translat 36 (2022) 83–90.
[51] Y. Xiong, Z. Lin, P. Bu, T. Yu, Y. Endo, W. Zhou, Y. Sun, F. Cao, G. Dai, Y. Hu, L. Lu, L. Chen, P. Cheng, K. Zha, M.A. Shahbazi, Q. Feng, B. Mi, G. Liu, A whole-course-repair system based on neurogenesis-angiogenesis crosstalk and macrophage reprogramming promotes diabetic wound healing, Adv. Mater. 35 (19) (2023), e2212300.
[52] J.A. Niska, J.A. Meganck, J.R. Pribaz, J.H. Shahbazian, E. Lim, N. Zhang, B. W. Rice, A. Akin, R.I. Ramos, N.M. Bernthal, K.P. Francis, L.S. Miller, Monitoring bacterial burden, inflammation and bone damage longitudinally using optical and muCT imaging in an orthopaedic implant infection in mice, PLoS One 7 (10) (2012), e47397.
[53] V.A. Stadelmann, I. Potapova, K. Camenisch, D. Nehrbass, R.G. Richards, T. F. Moriarty, In vivo MicroCT monitoring of osteomyelitis in a rat model, BioMed Res. Int. 2015 (2015), 587857.
[54] A. Ghimire, J.D. Skelly, J. Song, Micrococcal-nuclease-triggered on-demand release of vancomycin from intramedullary implant coating eradicates Staphylococcus aureus infection in mouse femoral canals, ACS Cent. Sci. 5 (12) (2019) 1929–1936.
[55] M. Wang, Y. Yang, K. Yuan, S. Yang, T. Tang, Dual-functional hybrid quaternized chitosan/Mg/alginate dressing with antibacterial and angiogenic potential for diabetic wound healing, J Orthop Translat 30 (2021) 6–15.
[56] H. Li, P. Yang, J. Hwang, P. Pageni, A.W. Decho, C. Tang, Antifouling and antimicrobial cobaltocenium-containing metallopolymer double-network hydrogels, Biomater Transl 3 (2) (2022) 162–171.
[57] F. Kang, Q. Yi, P. Gu, Y. Dong, Z. Zhang, L. Zhang, Y. Bai, Controlled growth factor delivery system with osteogenic-angiogenic coupling effect for bone regeneration, J Orthop Translat 31 (2021) 110–125.